# Branes Screening Quarks and Defect Operators

Andreas Karch[1] and Marcos Riojas[1,2]
[1]Weinberg Institute, Department of Physics, University of Texas, Austin, Texas 78712, USA
[2]Center for the Fundamental Laws of Nature, Harvard University, Cambridge, Massachusetts, USA

(Received 29 October 2025; revised 16 October 2026; accepted 26 October 2026; published 17 November 2026)

Here we show Wilson lines do not necessarily exhibit Coulomb scaling laws in AdS/BCFT at zero temperature. The area difference between a surface that returns to the boundary, and one that plunges into the bulk, determines the potential between two quarks. This classic AdS/CFT calculation is extended to Wilson surfaces associated to general $(p-1)$-form symmetries in boundary conformal field theories (BCFTs) by embedding a Karch-Randall (KR) brane. Work done on the boundary charge under a dilatation determines the coefficient of this potential in closed form. Consequently, Coulomb law scaling in subregion size $\Gamma$ is recovered only above the critical angle for the brane, $\theta_{c,p}$, where the configuration is dilatation invariant. The potential between the two quarks (or defect operators) vanishes precisely when the surface connecting them ceases to exist at $\theta_{c,p}$. Thus operators are fully screened in this phase transition from Coulomb law to perimeter law, for which we compute the order parameter $C_p$ of the transition. At finite temperature a horizon breaks dilatation invariance, and so $p$ analogs of islands continue to exist below $\theta_{c,p}$.

DOI: 10.1103/rx4t-twrx

*Introduction*—Subcritical Randall-Sundrum (RS) branes [1,2] with a cosmological constant, in this context also known as Karch-Randall (KR) branes, are practical bottom-up toy models of holographic duals for conformal field theories with boundaries (BCFTs) [1–4]. Particular emphasis has been placed in recent years on the calculation of entanglement entropies in these settings using the Ryu-Takayanagi (RT) prescription [5]; crucially, the codimension two extremal surfaces whose area determines entanglement entropy may attach to the KR brane.

It was recently realized that the brane induces a phase transition at late times between two classes of extremal surfaces when the field theory is effectively at finite temperature. This can be achieved for field theories by studying them in thermal equilibrium or by placing them on nondynamical black hole backgrounds. At early times the entanglement entropy grows linearly in time; from the holographic perspective, this is realized by a horizon-plunging Hartman-Maldacena (HM) surface [6]. The presence of the brane allows a time-independent class of saddles—known as island RT surfaces—to end on the brane instead of crossing the horizon. Thus the brane prevents the entanglement entropy from growing forever [7–12]. This behavior of the entanglement entropy has been interpreted as a generalized Page curve, by which we mean a time evolution consistent with unitarity.

In addition to the phase transition as a function of time these systems also exhibit a phase transition as a function of a control parameter governing the details of the BCFT [11,12], which from the bulk point of view is encoded in the angle between brane and boundary. Whether a nontrivial Page curve exists depends on whether the brane is above or below a critical angle. While this phenomenon is well established for RT surfaces, one of our novel findings is that the same phase transition also occurs for general $p$-dimensional minimal spatial surfaces in general $d+1$ dimensional locally asymptotically anti–de Sitter ($AdS_{d+1}$) spacetimes terminating on a KR brane. These minimal $p$-dimensional extremal objects have standard holographic duals: for $p=1$ (spacelike geodesics) they control two-point functions of large dimension operators; for $p=2$ (Euclidean string world sheets) they compute spatial Wilson and 't Hooft lines [13,14]; for $p \geq 3$ they realize the corresponding Wilson surface operators. In this way, the brane screens all $p-1$ dimensional defect operators, including Wilson lines ($p=2$).

Famous examples of probe branes for $p=2$ are F1 and D1 strings of type IIB string theory on $AdS_5 \times S^5$ which compute a Wilson and 't Hooft line, respectively, and differ only in their string tension $m$. For $p=3$ the M2 brane of M theory on $AdS_7 \times S^4$ calculates a surface observable in the dual (2,0) theory. Explicit top-down constructions realizing well-known BCFTs with very similar qualitative behavior [15–20] were shown [21] to exhibit the critical angle phenomenon. See Supplemental Material (SM) [22] for

*Published by the American Physical Society under the terms of the Creative Commons Attribution 4.0 International license. Further distribution of this work must maintain attribution to the author(s) and the published article's title, journal citation, and DOI. Funded by SCOAP³.*

additional discussion on this point. For $AdS_5$, a top-down ICFT with a tunable KR-like brane angle is realized by a probe D5-brane with nontrivial world volume flux [2,27], while its back reaction remains parametrically negligible. Reference [27] computed an interface-particle potential on both sides of this duality. A corresponding ICFT calculation of the general extended probes studied here is not presently known and generically difficult due to the strongly coupled nature of the dual CFT; our results give quantitative predictions for such a calculation.

Instead of a phase transition in entanglement entropy, for an interface conformal field theory (ICFT) this can be viewed as a phase transition in the potential between a quark and the boundary or, equivalently, between a quark and its mirror quark, or the analogous potential between a higher dimensional defect and the boundary for $p > 2$. For an ICFT this is a transition in the quark-antiquark potential, as depicted in Fig. 1. This is a higher dimensional generalization of the entanglement island formation previously seen in lower dimensions [28–30] based on the study of quantum entangling surfaces [31] in theories of gravity coupled to a bath.

In particular, at zero temperature—where the island forming phase transition may occur, even though it is not required by unitarity [10,11,32]—we find a simple universal pattern. The area of the minimal surface depends only on the surface dimension, $p$, and not on the number of bulk dimensions, $d$. At zero temperature the Page curve for the entanglement entropy in two-dimensional BCFTs (dual to subcritical RS branes) behaves identically to the two-point function of heavy operators for BCFTs of dimension $d$, the $d = 3$ Page curve gives the behavior of Wilson lines in any dimension, and so on for general $p$. This strongly suggests that BCFTs in general dimension $d$ experience phase transitions at the critical angles $\theta_{c,p}$ [11,12] for all $p \leq d-1$, provided there is an extended operator associated with this $p$ that can detect the transition.

This transition is a consequence of scaling under dilatations. Work is computed from boundary terms in the variation of the area functional, with $\tilde{z}$ as the independent variable. No work is done where the surface meets the brane, since the boundary condition is Neumann; it occurs at the bath anchor, where it is Dirichlet. The renormalized area results from pulling the anchor from infinity toward the interface; this energy difference is

$$A_p^{\mathrm{ren}} = -\frac{f_p(\theta_b)^p}{(p-1)\Gamma^{p-1}}, \qquad p > 1, \tag{1}$$

with $f_p$ given in (13) and $\Gamma$ the distance between the probe and the interface. There is a transition from Coulomb to perimeter law at the critical angle $\theta_{c,p}$ for the brane. The coefficient $C_p = f_p^p/(p-1)$ is the order parameter: it vanishes identically below $\theta_{c,p}$ and turns on as $(\theta_b - \theta_{c,p})^p$.

This result does not follow from scale invariance alone. Nonetheless, since $\Gamma$ is the only scale, the work done by displacing the boundary charge is fixed: $E \sim A_p^{\mathrm{ren}} \sim \Gamma^{1-p}$ and hence $\Gamma F = (p-1)|E|$, where $F \equiv \partial E/\partial\Gamma$. We show this follows from a direct computation of the work done on the boundary charge under a dilatation.

At finite temperature a horizon introduces a second scale and breaks dilatation invariance of the bulk action, and brane-anchored surfaces continue to exist below $\theta_{c,p}$. At $p = d-1$ islands below $\theta_{c,p}$ continue to produce a Page curve [11,12]; similarly, spatial Wilson surfaces of dimension $p$ may anchor on the brane below the critical angle, forming the analogs of islands and Page curves.

Finally, we give an elementary formula for the critical angle, which does not depend on temperature.

*The holographic calculation*—Here we are interested in minimal area submanifolds embedded in the purely spatial geometry of a constant time slice. The region of interest is the near-boundary geometry, i.e., empty $AdS_{d+1}$, so our results are broadly applicable to a wide variety of AdS spacetimes.

This is described by Poincare patch coordinates:

$$ds^2 = \frac{1}{\tilde{z}^2}(-dt^2 + d\vec{x_T}^2 + d\tilde{y}^2 + d\tilde{z}^2). \tag{2}$$

Translations along the defect directions and rotations around the surface insertion in the transverse $x_i$ directions are respected by these surfaces, which satisfy

$$t = 0, \qquad x_i = 0, \qquad \tilde{y} = \tilde{y}(\tilde{z}), \tag{3}$$

subject to the Dirichlet boundary condition that the surface is inserted at some point $\Gamma$, i.e., that $\tilde{y}(0) = \Gamma$. The KR brane is a ray through the origin, $\tilde{y} = -\tilde{z}\cot\theta_b$.

The action for such a minimal area embedding is

$$S = V_T m \int \frac{d\tilde{z}}{\tilde{z}^p}\sqrt{1 + (\tilde{y}')^2} \equiv V_T m A_p(\Gamma). \tag{4}$$

The $\tilde{z}$ dependence of the area density $A_p$ is independent of $d$ and depends only on $p$, the submanifold dimension. Here

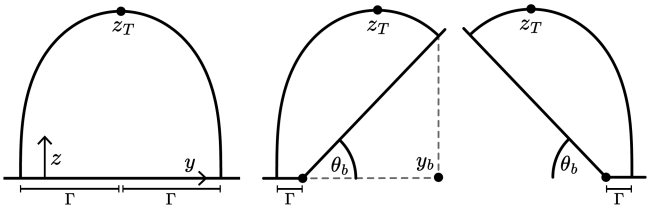



FIG. 1. The $p$-dimensional extremal surface dual to the closed Wilson surface $W(C)$ exhibits Coulomb law as $\Gamma \to 0$, both for empty AdS and at finite temperature. After a KR brane is introduced with angle $\theta_b$, the behavior as $\Gamma \to 0$ depends on whether $\theta_b$ is greater than or less than the critical angle $\theta_c$. Here we depict an ICFT rather than a BCFT to emphasize the close connection with the quark-antiquark potential.

$V_T$ is the volume of the surface in the transverse $\vec{x}$ directions. $A_p(\Gamma)$ denotes the actual area per unit transverse volume of the minimal surface anchored at $\tilde{y} = \Gamma$.

The meaning of $m$ depends on what we are calculating. For an RT surface, $m = (1/4G)$. The area diverges near the boundary and we write $A_p = \epsilon^{1-p}/(p-1) + A_p^{\rm ren}$. For most of the applications discussed in this work $m$ is a physical tension, and in such cases it is essential for our argument that we are in the "probe" regime, where $m$ is sufficiently small in Planck units to make the right-hand side of Einstein's equations negligible.

Since (4) does not depend on $\tilde{y}$, $P \equiv \partial\mathcal{L}/\partial\tilde{y}'$ is conserved. However, the Hamiltonian $H = P\tilde{y}' - \mathcal{L} = -[\tilde{z}^p\sqrt{1+(\tilde{y}')^2}]^{-1}$ is not: $dH/d\tilde{z} = -\partial\mathcal{L}/\partial\tilde{z} = (p/\tilde{z})\mathcal{L}$.

For computational convenience, consider the tangent angle $\psi$, measured from the downward vertical, so that the tangent vector satisfies $\mathbf{T} = (-\sin\psi, \cos\psi)$, where $\tilde{y}' = -\tan\psi$ and $\sqrt{1+(\tilde{y}')^2} = \sec\psi$, and so

$$P = -\frac{\sin\psi}{\tilde{z}^p}, \quad H = -\frac{\cos\psi}{\tilde{z}^p}, \quad P^2 + H^2 = \frac{1}{\tilde{z}^{2p}}. \tag{5}$$

At the turnaround point $z_T$, $H = 0$, so $|P| = z_T^{-p}$. Writing $ds = d\tilde{z}\sqrt{1+(\tilde{y}')^2}$, with $n(\tilde{z}) \equiv \tilde{z}^{-p}$, conservation of $P$ becomes Snell's law: $n\sin\psi = |P| = z_T^{-p}$. This gives

$$A_p = \int n\, ds, \qquad \sin\psi = \left(\frac{\tilde{z}}{z_T}\right)^p. \tag{6}$$

Differentiating (6) gives $d\tilde{z} = (z_T/p)\sin^{1/p-1}\psi\cos\psi d\psi$, hence $ds = (z_T/p)\sin^{1/p-1}\psi d\psi$. Then

$$\frac{dy}{d\psi} = -\frac{1}{p}\sin^{\frac{1}{p}}\psi, \qquad \frac{dA_p}{d\psi} = \frac{z_T^{1-p}}{p}\sin^{\frac{1}{p}-2}\psi, \tag{7}$$

where $y = \tilde{y}/z_T$. Note that $\psi$ runs monotonically from 0 at the anchor, through $\pi/2$ at the turnaround, so integrating through the turnaround is straightforward.

In terms of the tangent vector, $d\tilde{z} = \cos\psi ds$ and $d\tilde{y} = -\sin\psi ds$, so $n\mathbf{T} = (-\sin\psi, \cos\psi)\tilde{z}^{-p} = (P, -H)$ and the on-shell variation of the area is a pure boundary term,

$$\delta A_p = [n\mathbf{T}\cdot\delta\mathbf{X}]^{\rm brane}_{\rm anchor} = [P\delta\tilde{y} - H\delta\tilde{z}]^{\rm brane}_{\rm anchor}, \tag{8}$$

with $\mathbf{X} = (\tilde{y}, \tilde{z})$. No work is done at the KR brane due to the Neumann boundary condition (to be discussed below). Translating the endpoint on the boundary with $\delta\mathbf{X} = (\delta\Gamma, 0)$, since $P < 0$ the bracket gives $\delta A_p = |P|\delta\Gamma$. The counterterm is $\Gamma$ independent, which yields

$$\frac{\partial A_p^{\rm ren}}{\partial\Gamma} = |P|. \tag{9}$$

Work done on the boundary charge provides the energy needed to dilate the surface.

*The quark potential without branes*—First we show the standard calculation without branes, extending it to general $p$ when necessary. Without a brane the surface connects the $q\bar{q}$ pair symmetrically, with $\psi$ ranging from 0 at the boundary to $\pi/2$ at the turnaround. Integrating (7) from the boundary to the turnaround gives $\Gamma = z_T y_T$, where

$$y_T \equiv \frac{1}{p}\int_0^{\pi/2}\sin^{\frac{1}{p}}\psi d\psi = \frac{\sqrt{\pi}\,\Gamma\left(\frac{p+1}{2p}\right)}{\Gamma\left(\frac{1}{2p}\right)}. \tag{10}$$

If we were computing entanglement entropy, this would be the subregion size. The infinite part of the area arises from the quark masses; subtracting off the HM surface regulates the action, and the finite difference is the quark-antiquark potential, $V_{q\bar{q}} \equiv E = \mu A_p^{\rm ren}$ where $\mu \equiv mL^p V_{p-2}$. Since $|P| = z_T^{-p} = (y_T/\Gamma)^p$, (9) gives

$$A_p^{\rm ren} = -\frac{y_T z_T^{1-p}}{p-1} = -\frac{y_T^p}{(p-1)\Gamma^{p-1}} \sim \frac{1}{\Gamma^{p-1}}. \tag{11}$$

The $\Gamma^{1-p}$ scaling is Coulomb law [13,14]. For the special case of $p = 1$ the leading contribution goes like $\log(\Gamma)$.

*The quark potential with branes*—Here we introduce a KR brane and repeat the computation for the defect-boundary potential, which we will loosely continue to refer to as the quark-antiquark potential. The brane angle $\theta_b$ is a control parameter for the Wilson surface associated with the $(p-1)-$ form symmetry; we will demonstrate a transition from perimeter to Coulomb behavior at exactly $\theta_{c,p}$.

An endpoint now lies on the brane, where it slides along $\tilde{y} = -\tilde{z}\cot\theta_b$, so $\delta\tilde{y}_b = -\cot\theta_b\delta\tilde{z}_b$ and the corresponding term in (8) is $(-P\cot\theta_b - H)\delta\tilde{z}_b$. Since $H/P = \cot\psi_b$, by (6) this vanishes for arbitrary $\delta\tilde{z}_b$ iff

$$\psi_b = \pi - \theta_b, \qquad z_b^p = \sin\theta_b. \tag{12}$$

Here $z_b \equiv \tilde{z}_b/z_T$. The endpoint on the brane slides freely; no work is done, due to the standard (Neumann) boundary condition [10]. The tangent angle therefore runs from 0 at the anchor to $\pi - \theta_b$ at the brane, and $\theta_b = \pi/2$ recovers the mirror configuration of the previous subsection.

Through an analogous procedure, integrating (7) with $y_b = -\cos\theta_b\sin^{1/p-1}\theta_b$, (10) becomes

$$\Gamma = z_T\left(\frac{1}{p}\int_0^{\pi-\theta_b}\sin^{\frac{1}{p}}\psi d\psi + y_b\right) \equiv z_T f_p(\theta_b). \tag{13}$$

As illustrated in Fig. 2, $f_p(\theta)$ determines whether the extremal surface undershoots ($f_p(\theta) < 0$) or overshoots ($f_p(\theta) > 0$) the point at $z = 0$. If the surface undershoots the point at $z = 0$, no surface ending on the brane exists for

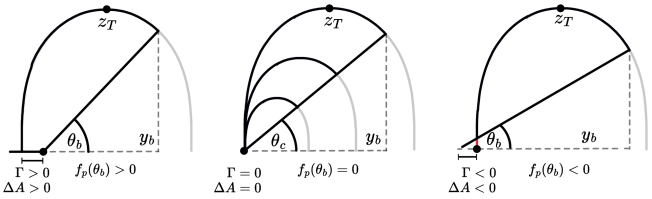



FIG. 2. The physical interpretation of $f_p(\theta)$ is that it determines whether the extremal surface undershoots ($f_p(\theta) < 0$) or overshoots ($f_p(\theta) > 0$) the defect at $\Gamma = 0$. On the LHS, above the critical angle, the surface overshoots the defect when $f_p(\theta) > 0$, which gives $\Gamma > 0$ and $A_p < 0$. In the middle, at the critical angle $\theta_{c,p}$, $f_p(\theta) = A_p = \Gamma = 0$. Dilatation invariance is manifest at the critical angle. On the RHS we are below the critical angle; we have $f_p(\theta) < 0$ and $\Gamma < 0$, so the brane-anchored surfaces cease to exist.

any $\Gamma$. This suggests the potential will vanish when $f_p(\theta) = 0$—we will find that it does, and we will uncover interesting behavior at this transition point.

Differentiating (13) gives

$$f_p'(\theta_b) = \frac{p-1}{p} \sin^{\frac{1}{p}-2} \theta_b > 0, \tag{14}$$

so $f_p$ is strictly monotonic. At fixed $\theta_b$ we have $|P| = z_T^{-p} = (f_p/\Gamma)^p$. For $p > 1$ an integration constant is forbidden by scaling in $\Gamma$; direct integration of (9) gives

$$A_p^{\text{ren}} = -\frac{f_p^p}{(p-1)\Gamma^{p-1}} = -\frac{|P|\Gamma}{p-1}. \tag{15}$$

Since $f_p(\pi/2) = y_T$, this contains (11) as a special case where the $Z_2$ symmetric brane has vanishing tension.

*Dilatations*—Alternatively, under the dilatation $\tilde{z} \to \lambda\tilde{z}$, $\tilde{y} \to \lambda\tilde{y}$, $\vec{x}_T \to \lambda\vec{x}_T$ we have $\delta\mathbf{X} = \alpha\mathbf{X}$, so (8) is $\alpha\mathcal{Q}$ with

$$\mathcal{Q} = n\mathbf{T}\cdot\mathbf{X} = P\tilde{y} - H\tilde{z}, \qquad \frac{d\mathcal{Q}}{d\tilde{z}} = (1-p)\mathcal{L}, \tag{16}$$

where we used $dP/d\tilde{z} = 0$, the nonconservation of $H$, and $P\tilde{y}' - H = \mathcal{L}$. Substituting (5) gives $\mathcal{Q} = -|P|b$ with $b \equiv \tilde{y} - \tilde{z}\cot\psi$, the point where the normal at $\psi$ meets the boundary. At the brane the normal lies along the KR brane, which passes through the origin, so $b(\psi_b) = 0$ and $\mathcal{Q}_{\text{brane}} = 0$, which is consistent with the Neumann boundary condition. Work is done at the boundary: $\tilde{y} \to \Gamma$ as $\psi \to 0$ and $\tilde{z}\cot\psi = z_T^p \tilde{z}^{1-p} + \mathcal{O}(\tilde{z}^{1+p})$, so $\mathcal{Q}(\epsilon) = -|P|\Gamma + \epsilon^{1-p}$. Then (16) immediately gives

$$A_p^{\text{ren}} = \frac{\mathcal{Q}_{\text{brane}} - \mathcal{Q}_{\text{anchor}}^{\text{ren}}}{1-p} = -\frac{|P|\Gamma}{p-1}, \tag{17}$$

with $E = \mu A_p^{\text{ren}}$ and $F = \mu|P|$, where $\mu \equiv mL^p V_{p-2}$,

$$\Gamma F = (p-1)|E|. \tag{18}$$

Work done by translating the boundary anchor provides the energy needed to dilate the surface. This work vanishes at the critical angle by dilatation invariance.

Note that $E = \mu A_p^{\text{ren}} < 0$ is the binding energy between the two quarks; $F = \mu|P|$ holds them apart.

*The critical angle*—Since $\Gamma = z_T f_p$, the condition $f_p(\theta_{c,p}) = 0$ yields $\Gamma = A_p^{\text{ren}} = 0$ for every $z_T$, a consequence of dilatation invariance manifest in the middle panel of Fig. 2.

Using $f_p(\theta_{c,p}) = 0$ and $f_p(\pi/2) = y_T$ from (10), and integrating $f_p'$ in (14) yields an equation for $\theta_{c,p}$:

$$\frac{p-1}{p}\int_{\theta_{c,p}}^{\pi/2} \sin^{\frac{1}{p}-2}\theta\, d\theta = y_T = \frac{\sqrt{\pi}\,\Gamma\left(\frac{p+1}{2p}\right)}{\Gamma\left(\frac{1}{2p}\right)}. \tag{19}$$

This generalizes and streamlines our previous result [11], allowing us to prove several statements. The left side decreases monotonically from $+\infty$ to 0 as $\theta_{c,p}$ runs from 0 to $\pi/2$, since $(1/p) - 2 < -1$ for $p > 1$. The uniqueness and existence properties observed in [11] follow immediately. At fixed $\theta_{c,p}$ the left side increases with $p$ while the right side decreases; $d\theta_{c,p}/dp > 0$, which gives

$$\theta_{c,1} = 0 < \theta_{c,2} < \cdots < \theta_{c,d-1}. \tag{20}$$

The monotonicity of the critical angle was a numerical result of [11]. Equation (19) gives the asymptotic expansion

$$\theta_{c,p} = \frac{\pi}{2} - \frac{\pi}{2p} - \frac{\pi(1-\ln 2)}{2p^2} + \mathcal{O}(p^{-3}). \tag{21}$$

This value is unchanged at finite temperature [11].

Coulomb law goes unrealized below $\theta_{c,p}$ because the surfaces, which can no longer satisfy the Neumann boundary condition, cease to exist. This is perimeter law because the potential between quark (or defect) and boundary does not depend on the distance to the boundary when the brane lies below the critical angle $\theta_{c,p}$. Although this resulted from the boundary condition, this is in fact a physical requirement for the BCFT to be self-consistent, because $f_p(\theta) < 0$ would give *positive* binding energy $E = \mu A_p^{\text{ren}} > 0$ between the mirror quarks.

With $A_p^{\text{ren}} \equiv -C_p/\Gamma^{p-1}$ and $f_p \simeq f_p'(\theta_{c,p})(\theta_b - \theta_{c,p})$,

$$C_p = \frac{f_p(\theta_b)^p}{p-1} \simeq \frac{(p-1)^{p-1}}{p^p} \sin^{1-2p}\theta_{c,p}(\theta_b - \theta_{c,p})^p. \tag{22}$$

This transition from Coulomb law above $\theta_{c,p}$ to perimeter law below $\theta_{c,p}$, where $C_p$ is the order parameter for the transition and $p$ is the critical exponent, is one of the primary results of this Letter. Many aspects of this

transition are universal, as they apply to the near-boundary region in every asymptotically AdS geometry.

We emphasize that although conformal invariance fixes the power of $\Gamma$ in the renormalized interaction, that does not determine its coefficient, and also does not forbid that coefficient from vanishing. Our result is the prediction that it vanishes over a finite range of interface parameters and that its order parameter satisfies $C_p \propto (\theta_b - \theta_{c,p})^p$.

*Screening at finite temperature*—Here we show that Coulomb law is not realized below the critical angle at finite temperature. The simplest way to extend our results to theories at finite temperature is to place the field theory on a nondynamical black hole background, where a position-dependent finite temperature emerges because the field theory Hawking radiates.

For simplicity we use the "planar black string" metric for our bulk geometry, where $u_h$ is the horizon radius:

$$ds^2 = \frac{1}{u^2 \sin^2\mu}\left[-h(u)dt^2 + \frac{du^2}{h(u)} + u^2 d\mu^2 + d\vec{x}^2\right],$$

where $h(u) = 1 - (u^{d-1}/u_{\rm h}^{d-1})$ and $u \equiv (1/r)$ is measured from the boundary of AdS. For the zero temperature case, there was degeneracy between different $d$ for the same $p$; this is clearly broken at finite temperature.

In the field theory we are still looking at time independent configurations parallel to the defect; in the $u-\mu$ coordinates we want $u = u(\mu)$ with $u(\pi) = \Gamma$. In this finite temperature case the degeneracy between spacelike and timelike surfaces is *also* broken. For a spacelike surface we take, as before, $t = 0$ and $x_i = 0$. Then

$$A = V \int \frac{d\mu}{[u \sin\mu]^p} \sqrt{\frac{(u')^2}{h[u]} + u^2}. \tag{23}$$

For temporal Wilson surfaces, the timelike surface treats one more of the $x_i$ as a transverse coordinate, which simply introduces an extra factor of $\sqrt{h(u)}$ into the action.

Figure 3 shows extremal surfaces that may end on the KR brane at a critical anchor $u_b$. Coulomb scaling occurs only when the brane satisfies $\theta_b > \theta_{c,p}$; the resulting surfaces shrink to infinitesimal size as $\Gamma \to 0$. Otherwise the saddle attaches at finite $u_b$ with $u_b \to 0$ as $\theta \to \theta_{c,p}$. Figures, boundary conditions, and additional details can be found in Supplemental Material (SM) [22].

*The area difference at the critical angle*—For the black string the HM surface is nontrivial; the area of the HM surface anchored to the defect must be computed for generic $p$ and $d$ at finite temperature. This suffices to determine the area difference at the critical angle for $\Gamma = 0$ because the regulated area of a surface shrinking into the defect vanishes, i.e. $\Delta A_c = -A_{HM}$.

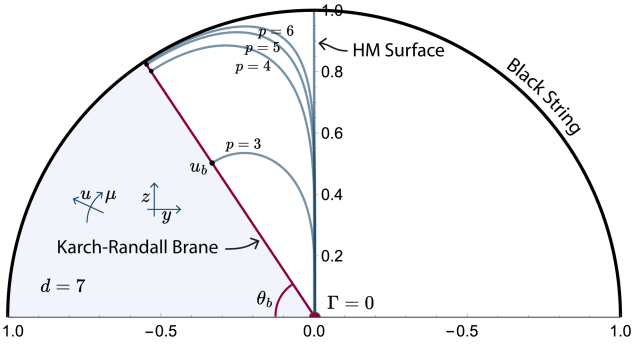



FIG. 3. The behavior at the critical angle $\theta_{c,p}$ at finite temperature for $p$-dimensional extremal surfaces dual to $p-1$ dimensional defect operators. The background geometry is the $d = 7$ dimensional black string. Spatial Wilson surfaces at $\Gamma = 0$ touch the brane at the critical anchor $u_b$. Note $\theta_b$ is slightly below the critical angle for $p = 3$ surfaces ($\theta_{c,3} \approx .98687$), and above $\theta_{c,1}$ and $\theta_{c,2}$. The $p = 1$ and $p = 2$ dimensional surfaces have vanishing critical anchors, and hence (generalized) Coulomb law scaling as $\Gamma \to 0$.

For a spatial Wilson line the area functional reads,

$$A = \int \frac{du}{(u \sin\mu)^p} \sqrt{u^2 \mu'(u)^2 + \frac{1}{h(u)}}. \tag{24}$$

The HM surface plunges directly into the black hole when $\Gamma = 0$, so $\mu'(u) = 0$. Since $\mu = \pi/2$ along its trajectory, the area of the HM surface is

$$A_{HM} = \int_0^1 \frac{dz}{z^p}\left(\sqrt{\frac{1}{h(z)}}\right). \tag{25}$$

For the planar AdS black hole we have $h(z) = 1 - z^{d-1}$.

We regulate this formally divergent integral by a change of variables adapted to the black-hole shadow. For an observer at a distance $r_0$ from the photon ring at $r_{\rm ps}$, the angular extent $\alpha$ of the black hole shadow is $\sin(\alpha) = \sqrt{(h(r_0)/h(r_{\rm ps}))}$. For the photon ring in our setup, an observer located on the slice along the HM surface is a distance $z$ from the photon ring at the AdS boundary:

$$\csc(\alpha) = \sqrt{\frac{1}{h(z)}}. \tag{26}$$

This coordinate transformation applied to (25) gives $A_{HM} = 2/(d-1)\int_0^{\pi/2} \cos(\alpha)^n d\alpha$, where $n = 2[(1-p)/(d-1)] - 1$. For analytical continuation in $n$, the integral is simply $\int_0^{\pi/2} \cos(\alpha)^n d\alpha = \{\sqrt{\pi}\Gamma[(n+1)/2]/2\Gamma[(n/2)+1]\}$. Then $\Delta A$ at $\theta_{c,p}$ is

$$\Delta A_c = -A_{HM} = \frac{\sqrt{\pi}}{1-d}\frac{\Gamma\left(\frac{1-p}{d-1}\right)}{\Gamma\left(\frac{1-p}{d-1}+\frac{1}{2}\right)}. \tag{27}$$

This is infinite when $(p-1)/(d-1)$ is an integer and vanishes when $(p-1)/(d-1)$ is a half integer. Since $1 < p < d$ for all solutions of interest this integral is finite. This expression is verified numerically in SM [22]. The critical angle vanishes as $p \to 1$; the counterterm $1/(p-1)$ gives $\Delta A_{c,p=1} = \log(4)/(1-d)$.

For the temporal Wilson surface the calculation is elementary and gives $\Delta A_c^{\tau} = u_h^{1-p}(p-1)^{-1}$.

*Discussion*—In this Letter we used Karch-Randall (KR) branes to screen the potential between quarks and extended this to include $p-1$ dimensional defect operators. Thus the important result that Wilson lines and surfaces exhibit Coulomb scaling laws in AdS/CFT at zero temperature [13,14] does not necessarily hold for BCFTs. The force between the quarks vanishes at a critical angle for the brane $\theta_{c,p}$ and a transition occurs from Coulomb law to perimeter law, with $C_p$ acting as an order parameter. This holds for RT surfaces and for $p-1$ dimensional defect operators in ICFTs and BCFTs. Because $\theta_{c,p}$ increases with $p$, a fixed theory has nested screening regimes. It is unexpected that $\theta_{c,p}$ and the critical transition depend only on $p$, and not on $d$; this is a universal connection linking seemingly unrelated quantities across dimensions.

At finite temperature a regularization technique inspired by the photon ring gave closed-form expressions for divergent integrals. This determined the action at finite temperature at $\theta_{c,p}$ for $p-1$ dimensional defect operators. Work is done under dilatations because the horizon breaks the scale invariance of the bulk action.

*Acknowledgments*—Special thanks to Jacques Distler and Amir Raz for critical questions and useful discussions. M. R. also thanks Hao-Yu Sun and Zixia Wei for helpful comments. The revised version of this work performed some calculations with assistance from GPT 5.6 and Claude 4.8. This work was supported, in part, by the US Department of Energy under Grant No. DE-SC0022021 and by a grant from the Simons Foundation (Grant No. 651678, A. K.). M. R. was also supported by a Dissertation Fellowship from CNS, an OGS Summer Fellowship, the Dean's Strategic Fellowship, and the GRASP initiative at Harvard University.

*Data availability*—The data that support the findings of this article are openly available, embargo periods may apply.

[1] A. Karch and L. Randall, J. High Energy Phys. 05 (2001) 008.
[2] A. Karch and L. Randall, J. High Energy Phys. 06 (2001) 063.
[3] T. Takayanagi, Phys. Rev. Lett. **107**, 101602 (2011).
[4] M. Fujita, T. Takayanagi, and E. Tonni, J. High Energy Phys. 11 (2011) 043.
[5] S. Ryu and T. Takayanagi, Phys. Rev. Lett. **96**, 181602 (2006).
[6] T. Hartman and J. Maldacena, J. High Energy Phys. 05 (2013) 014.
[7] A. Almheiri, R. Mahajan, J. Maldacena, and Y. Zhao, J. High Energy Phys. 03 (2020) 149.
[8] A. Almheiri, R. Mahajan, and J. E. Santos, SciPost Phys. **9**, 001 (2020).
[9] H. Geng and A. Karch, J. High Energy Phys. 09 (2020) 121.
[10] H. Z. Chen, R. C. Myers, D. Neuenfeld, I. A. Reyes, and J. Sandor, J. High Energy Phys. 10 (2020) 166.
[11] H. Geng, A. Karch, C. Perez-Pardavila, S. Raju, L. Randall, M. Riojas, and S. Shashi, SciPost Phys. **10**, 103 (2021).
[12] H. Z. Chen, R. C. Myers, D. Neuenfeld, I. A. Reyes, and J. Sandor, J. High Energy Phys. 12 (2020) 025.
[13] J. M. Maldacena, Phys. Rev. Lett. **80**, 4859 (1998).
[14] S.-J. Rey and J.-T. Yee, Eur. Phys. J. C **22**, 379 (2001).
[15] E. D'Hoker, J. Estes, and M. Gutperle, J. High Energy Phys. 06 (2007) 022.
[16] E. D'Hoker, J. Estes, and M. Gutperle, J. High Energy Phys. 06 (2007) 021.
[17] O. Aharony, L. Berdichevsky, M. Berkooz, and I. Shamir, Phys. Rev. D **84**, 126003 (2011).
[18] B. Assel, C. Bachas, J. Estes, and J. Gomis, J. High Energy Phys. 08 (2011) 087.
[19] D. Gaiotto and E. Witten, J. Stat. Phys. **135**, 789 (2009).
[20] C. Bachas and I. Lavdas, J. High Energy Phys. 11 (2018) 003.
[21] C. F. Uhlemann, J. High Energy Phys. 08 (2021) 104.
[22] See Supplemental Material at http://link.aps.org/supplemental/10.1103/rx4t-twrx for derivations, boundary conditions, numerics, and extra figures. It includes Refs. [23–26].
[23] S. Demulder, A. Gnecchi, I. Lavdas, and D. Lust, J. High Energy Phys. 02 (2023) 016.
[24] H. Geng, A. Karch, C. Perez-Pardavila, S. Raju, L. Randall, M. Riojas, and S. Shashi, J. High Energy Phys. 01 (2022) 182.
[25] A. Karch, C. Perez-Pardavila, M. Riojas, and M. Youssef, J. High Energy Phys. 05 (2023) 195.
[26] C. R. Graham and E. Witten, Nucl. Phys. **B546**, 52 (1999).
[27] K. Nagasaki, H. Tanida, and S. Yamaguchi, J. High Energy Phys. 01 (2012) 139.
[28] A. Almheiri, N. Engelhardt, D. Marolf, and H. Maxfield, J. High Energy Phys. 12 (2019) 063.
[29] G. Penington, J. High Energy Phys. 09 (2020) 002.
[30] A. Almheiri, T. Hartman, J. Maldacena, E. Shaghoulian, and A. Tajdini, Rev. Mod. Phys. **93**, 035002 (2021).
[31] N. Engelhardt and A. C. Wall, J. High Energy Phys. 01 (2015) 073.
[32] H. Geng, A. Karch, C. Perez-Pardavila, S. Raju, L. Randall, M. Riojas, and S. Shashi, J. High Energy Phys. 05 (2022) 153.